

PAPER • OPEN ACCESS

How patchiness controls the properties of chain-like assemblies of colloidal platelets

To cite this article: Carina Karner *et al* 2020 *J. Phys.: Condens. Matter* **32** 204001

View the [article online](#) for updates and enhancements.

You may also like

- [Platelet size and density affect shear-induced thrombus formation in tortuous arterioles](#)
Jennifer K W Chesnutt and Hai-Chao Han
- [Magnetically induced elastic deformations in model systems of magnetic gels and elastomers containing particles of mixed size](#)
Lukas Fischer and Andreas M Menzel
- [Computer simulations of self-assembly of anisotropic colloids](#)
Sriram Krishnamurthy, Remya Ann Mathews Kalapurakal and Ethayaraja Mani

How patchiness controls the properties of chain-like assemblies of colloidal platelets

Carina Karner^{1,2}, Christoph Dellago¹ and Emanuela Bianchi^{2,3}

¹ Faculty of Physics, University of Vienna, Boltzmannngasse 5, A-1090, Vienna, Austria

² Institut für Theoretische Physik, TU Wien, Wiedner Hauptstraße 8-10, A-1040 Wien, Austria

³ CNR-ISC, Uos Sapienza, Piazzale A. Moro 2, 00185 Roma, Italy

E-mail: carina.karner@univie.ac.at and emanuela.bianchi@tuwien.ac.at

Received 15 October 2019, revised 6 December 2019

Accepted for publication 21 January 2020

Published 18 February 2020



Abstract

Patchy colloidal platelets with non-spherical shapes have been realized with different materials at length scales ranging from nanometers to microns. While the assembly of these hard shapes tends to maximize edge-to-edge contacts, as soon as a directional attraction is added—by means of, e.g. specific ligands along the particle edges—a competition between shape and bonding anisotropy sets in, giving rise to a complex assembly scenario. Here we focus on a two-dimensional system of patchy rhombi, i.e. colloidal platelets with a regular rhombic shape decorated with bonding sites along their perimeter. Specifically, we consider rhombi with two patches, placed on either opposite or adjacent edges. While for the first particle class only chains can form, for the latter we observe the emergence of either chains or loops, depending on the system parameters. According to the patch positioning—classified in terms of different configurations, topologies and distances from the edge center—we are able to characterize the emerging chain-like assemblies in terms of length, packing abilities, flexibility properties and nematic ordering.

Keywords: colloidal platelets, patchy colloids, colloidal polymers, self-assembly

 Supplementary material for this article is available [online](#)

(Some figures may appear in colour only in the online journal)

1. Introduction

The interest in the self-assembly of colloidal chains stems from a variety of different applications. On one hand, colloidal chains can be seen as larger-scale version of linear polymers and, thus, they can serve as model systems to investigate the chain dynamics: the advantage of colloidal chains with respect to polymers and biopolymers is that they can be observed on a single-particle level in real space with optical techniques [1, 2]. As, for instance, the flexibility of colloidal chains can be tuned from the rigid to the semi-flexible down to the flexible regime [2], its effect on the dynamics in the response to an external field can be investigated [3], thus providing insights

on natural phenomena—such as flagellar motion [4] or conformational transitions in polymer systems [5]—as well as on how to fabricate and optimize microfluidic devices [6]. On the other hand, colloidal chains are *per se* applicable, e.g. as microscale detectors [7, 8], responsive materials with optical properties [9] and wavy arrays of self-assembled colloidal fibres for specific functionalization or coating [10].

The emergence of linear assemblies usually relies on directional interactions. Anisotropic interactions can be introduced, for instance, through the application of external electric or magnetic fields [11] or via the design of interaction patterns generated by well-defined bonding sites, also referred to as ‘patches’ [12–14]. In the first case, external fields induce a dipole moment that leads to a preferred assembly along the direction of the applied field. As the resulting chains disassociate to individual particles when the fields are switched off, an extra experimental step is needed to permanently link

 Original content from this work may be used under the terms of the [Creative Commons Attribution 4.0 licence](#). Any further distribution of this work must maintain attribution to the author(s) and the title of the work, journal citation and DOI.

the connected particles [2]. The field-directed assembly can also be used to assemble structures from non-spherical particles; in this case, the assembly is governed by two factors: the polarization of particles and the entropic interactions related to the particle shape [15–17]. In contrast, patchy colloids can provide directional interactions even in the absence of an external field [12–14]. Colloidal patchy polymers have been for instance studied to investigate and reproduce the folding of proteins at micrometer scale [18]. We note that, solid patches are typically used but liquid patches are also a viable way to induce one-dimensional assembly [19]. The two approaches—patches and external fields—can be combined, thus producing interesting responsive materials for application in, e.g. micro-robotics [20, 21].

Here we study the formation of chain-like assemblies emerging in two-dimensional systems of non-spherical patchy particles. Colloidal platelets of different shapes can be realized experimentally at the nano- up to the micro-scale: polygonal truncated silica pyramids, lanthanide fluoride nanocrystals and DNA-origami of several shapes are just a few examples [22, 23]. Additional directionality in bonding can be imparted to the systems by, e.g. covering the colloidal edges with ligands [24] or immersing them in a liquid crystal medium [25]. While hard shapes assemble by maximizing their edge-to-edge contacts, the additional bonding pattern induced by the patches favors configurations where the number of bonds can be maximized.

In our investigation, we consider rhombic platelets decorated with two attractive patches in various geometries: patches can be placed either on opposite or adjacent edges. Within these two big classes of systems, we explore the assembly scenario resulting from different patch positioning, focusing on those where chain-like assembly prevails.

The paper is organized as follows: in section 2 we describe the patchy rhombi model (section 2.1) and provide the details of our two-dimensional Monte Carlo simulations (section 2.2), in section 3 we discuss our results, first for systems where only chains can form (section 3.1) and then for systems where chains compete with loops and micelles (section 3.2). Finally in section 4 we draw our conclusions.

2. Model and methods

2.1. Particle model

Our particles are regular hard rhombi (see the sketch in figure 1) with two attractive square-well interaction sites, denoted as patches in the following and placed on different edges. In general the interaction potential between two hard particles i and j is given by

$$U(\vec{r}_{ij}, \Omega_i, \Omega_j) = \begin{cases} 0 & \text{if } i \text{ and } j \text{ do not overlap} \\ \infty & \text{if } i \text{ and } j \text{ do overlap.} \end{cases}$$

with \vec{r}_{ij} as the center-to-center distance vector, and Ω_i and Ω_j as particle orientations. To determine the overlaps between the rhombi we employ the separating axis theorem for convex

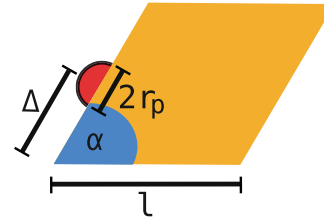


Figure 1. Rhombic platelet with one patch: the side length l sets the unit length, the opening angle $\alpha = 60^\circ$ for a regular rhombus, the patch diameter $2r_p = 0.1$, as in table 1. The patch position is determined by the parameter Δ , as labeled.

polygons, detailed in [26]. The patch-patch potential is of square-well type defined by

$$W(p_{ij}) = \begin{cases} -\epsilon & \text{if } p_{ij} < 2r_p \\ 0 & \text{if } p_{ij} \geq 2r_p, \end{cases}$$

where p_{ij} is the patch–patch distance, $2r_p$ is the patch diameter and ϵ denotes the patch interaction strength. A patchy rhombi model of this kind was first introduced in [27], with four attractive patches placed in the center of the edges.

Regular rhombi with two patches can be classified in three configuration types, as there are three ways to distribute two patches on four edges: first, patches can be placed on opposite edges—a configuration referred to as parallel (pl)—secondly, patches can be placed to enclose the big angle—a configuration denoted as manta (ma)—and thirdly, patches can be placed to enclose the small angle—a configuration denoted as mouse (mo). For a sketch of pl-class see the top of figure 2, for ma- and mo- systems see the top of figure 5. In each particle class, patches can be placed anywhere on their respective edges, resulting in an—in principle—infinite number of possible patchy rhombi. To study these systems methodically and give instructive design directions we introduce symmetric and asymmetric patch topologies. Patch topologies—or movement patterns—prescribe how to move the patches with respect to each other when scanning the parameter space. In the symmetric (s) topology, patches are always placed symmetrical with respect to their enclosing vertex (ma- and mo-systems) or such that patches on opposing edges sit exactly opposite to each other (pl-systems). In contrast, in the asymmetric (as) topology, patches are placed asymmetrically with respect to the enclosing angle (ma- and mo-systems) or such that the patch positions are mirrored with respect to the edge center (pl-systems). Note that it suffices to state the relative position Δ of only one of the two patches with respect to the reference vertex, as the second one is automatically defined through the choice of topology (see figures 2 and 5). With these definitions a two-patch system is fully defined through its patch configuration (pl, ma or mo), its topology (s or as) and its relative position on the edge (Δ). It is important to note that in the edge-center, i.e. at $\Delta = 0.5$, the s- and as-topology collapse into the center topology and the respective systems are denoted as pl-, ma- and mo-center systems. A summary of the used particle parameters can be found in table 1 and figure 1. We note that, for pl-systems we show results up to

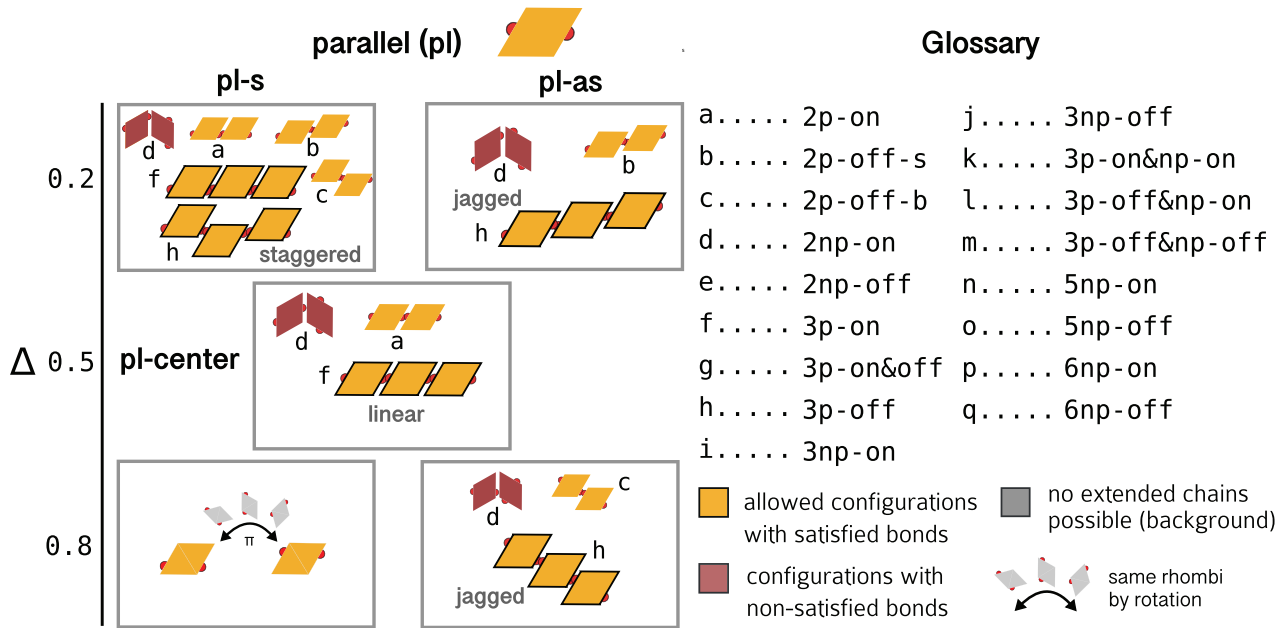


Figure 2. Left: small cluster analysis for parallel (pl) systems; left column: symmetric topology (pl-s), right column: asymmetric topology (pl-as), as labeled. The row corresponds to $\Delta = 0.2$ (top), 0.5 (center) and 0.8 (bottom), as labeled. Note that at $\Delta = 0.5$, both pl-s and pl-as collapse to pl-center. Clusters with fully bonded rhombi are colored in orange, while clusters with non-satisfied bonds are colored in burgundy. Note that pl-s with $\Delta = 0.2$ and pl-s with $\Delta = 0.8$ yield the same system by rotation of π , while pl-as are not symmetric with respect to $\Delta = 0.5$. Right: glossary of cluster labels. Dimers with on-edge parallel bonds (2p-on) are labeled with a, dimers with off-edge parallel bonds (2p-off) are labeled with either b (off-edge bonds closer to the small angle, 2p-off-s) or c (off-edge bonds closer to the big angle, 2p-off-b), dimers with non-parallel bonds (2-np) are labeled with either d (on-edge bonds, 2-np-on) or e (off-edge bonds, 2-np-off). The same logic applies to trimers and bigger clusters.

Table 1. Single particle parameters. See figure 1 for a graphical representation of the edge length l , the opening angle α , the patch radius r_p and the patch position parameter Δ .

Parameter	Symbol	Value
Angle	α	60°
Side length	l	1.0
Patch radius	r_p	0.05
Interaction strength	ϵ	5.2–10.2
Patch position	Δ	0.2–0.8

$\epsilon = 8.2k_B T$, where particles mostly belong to chains, while for ma- and mo-systems we show only $\epsilon = 10.2k_B T$, as at lower attraction strengths the competition with other assembly products plays a non-negligible role. For an extensive discussion about the ϵ -dependent behavior of ma- and mo-systems out of the chain regime we refer to [28].

2.2. Simulation details

We model the adsorption of the platelets on a surface with grand canonical (μVT ensemble) simulations with single particle rotation and translation moves and particle insertion and deletion. Cluster moves are added to avoid kinetic traps [29, 30]. All systems are initially equilibrated for 3×10^5 MC-sweeps at very low packing fraction ($\phi \approx 0.05$) with a fixed chemical potential μ_{eq} . After equilibration, we increase the chemical potential to μ^* to observe the assembly. We performed eight simulation runs per system and interaction strength ϵ . We note that for all center systems we collected twice the statistics

Table 2. The system parameters used in all simulations.

System parameter	Symbol	Value
Area of simulation box	A	$1000 \cdot \sin(60^\circ)$
Box width	L_x	$\sqrt{1000}$
Box height	L_y	$\sqrt{1000} \cdot \sin(60^\circ)$
Chemical potential to equilibrate	μ_{eq}	0.1
Chemical potential	μ^*	0.3
Boltzmann constant	k_B	1
Temperature	T	0.1

as we run both s- and as-topologies with $\Delta = 0.5$; most of the analysis is performed by considering these two data sets as independent, but of course they yield the same results. For ma- and mo-systems, we run the simulations for about $\approx 3 \times 10^6 - 5.0 \times 10^6$ MC-sweeps before collecting statistics. Pl-systems assembled faster and the total duration of the runs is $\approx 1 \times 10^6$ MC-sweeps. We note that although a single simulation run is not very expensive— 1×10^6 MC-sweeps take ≈ 36 hrs—the number of core hours amounts to a total of ≈ 60000 hrs as we performed an extensive study of the parameter space (ϵ, Δ) for all topologies and particle classes. The system parameters for all simulations are given in table 2.

3. Results

In general, on varying the patch positioning Δ and the patch-patch interaction strength ϵ , two-patch rhombi yield three different classes of self-assembly products: chains, loops

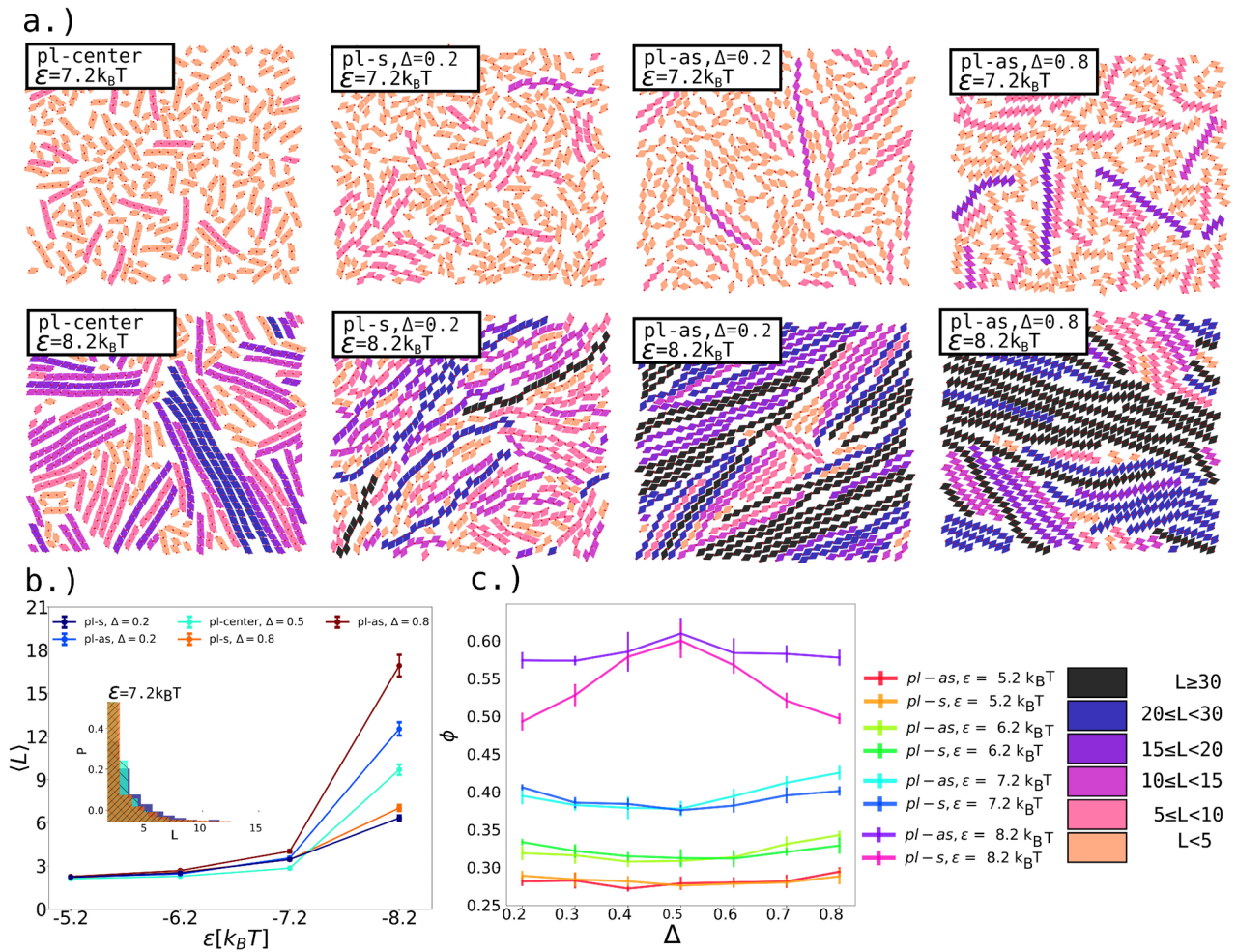


Figure 3. (a) Snapshots of pl-center (first column, linear chains), pl-s (second column, staggered chains) and pl-as (third and fourth columns, jagged chains) colored according to the chain length (see color scale at the bottom) for interactions strengths $\epsilon = 7.2 k_B T$ (top row) and $\epsilon = 8.2 k_B T$ (bottom row). While pl-s-rhombi with $\Delta = 0.2$ and $\Delta = 0.8$ are the same by rotation of π , pl-as-rhombi form two types of jagged chains: for $\Delta = 0.2$ particles bond off-edge with the bonds closer to the small rhombi angle, while for $\Delta = 0.8$ particles bond off-edge with the bonds closer to the big rhombi angle. (b) Average chain lengths (L) of pl-systems (as labeled) as function of interaction strength ϵ . The error bars were calculated with the standard error of the mean. Inset: distribution of chain length for $\epsilon = 7.2 k_B T$ for all pl-systems, as labeled. (c) Packing fraction ϕ of pl-systems as function of the patch position Δ at different interaction strengths ϵ .

and micelles, where micelles can be defined as minimal loops. While pl-systems form chains for any Δ and ϵ value, ma- and mo-systems form chains, loops and micelles. In our discussion we mostly focus on characterizing and comparing the emerging chains in different systems and we postpone the analysis of the emerging loops and micelles in ma- and mo-systems to [28]. The different assembly scenarios result from the interplay between steric constraints and patchiness. By construction, our patchy rhombi can form only one bond per edge, for a total of two bonds per particle. A pair of such rhombi can bind in two possible orientations: parallel (p)—i.e. with their long axes oriented parallel to each other—and non-parallel (np)—i.e. with their long axes in an arrowhead orientation. It is worth noting already at this stage that micelles contain only np-bonds, while loops need both p- and np-bonds and chains must contain p-bonds but can accommodate np-bonds.

3.1. Chains in pl-systems

We start our discussion with the analysis of pl-systems. As anticipated, all pl-systems, namely pl-center, pl-s and pl-as, form p-bonded chains for all choices of Δ and ϵ . This observation can already be deduced from the small cluster analysis reported in figure 2: this analysis determines which clusters can form depending on system type, topology and patch position. In pl-systems the patch positioning is not compatible with np-bonds (see dimers referred to as d in all panels of figure 2) and thus pl-rhombi can assemble only in chains (see configurations referred to as f and h), with either on-edge (configurations a) or off-edge (configurations b and c) p-bonds. In particular, chains in the pl-center topology consist exclusively of on-edge bonds, pl-as have only off-edge bonds and pl-s chains can have both. These bonding constraints lead to chain types that differ from each other in appearance as well as in physical properties. The on-edge bonds of pl-center

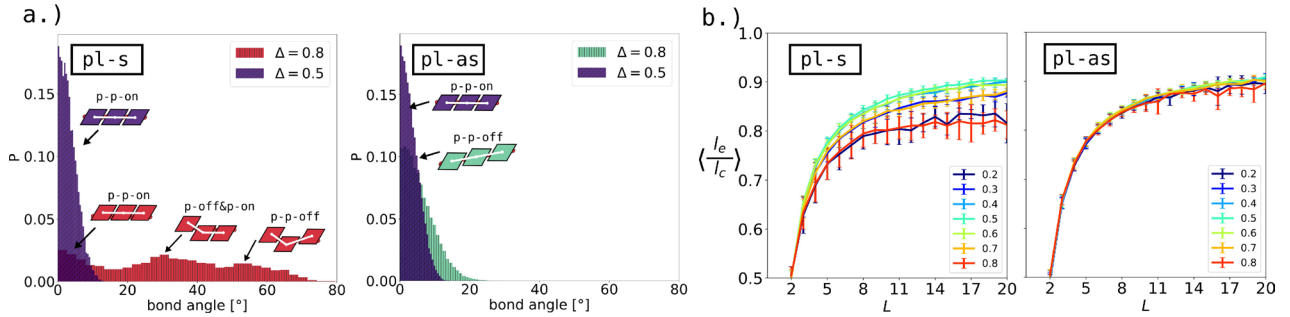


Figure 4. (a) Distribution of bond angles for pl-center (blue), pl-s (red) and pl-as (green). Sketches of bonding configurations corresponding to the peaks are added in corresponding colors. The naming scheme of such a configuration takes into account if bonds are parallel or non-parallel as well as if bonds are on- or off-edge, namely ‘p-p’: two parallel bonds; ‘p-np’: one parallel and one non-parallel bond; ‘np-np’: two non-parallel bonds; ‘on’: on-edge bonds, ‘off’ off-edge bonds. (b) The average ratio between the end-to-end distance l_e and the contour length l_c , $\langle l_e/l_c \rangle$, for pl-s (left) and pl-as (right), as function of the chain length L and for different Δ -values.

result in *linear* chains, the off-edge bonds of pl-as leads to *jagged* chains and the mix of on-edge and off-edge bonds in pl-s yields *staggered* chains (see figure 2 for small clusters and figure 3(a) for simulation snapshots). It is important to note that there are two different types of jagged chains: for $\Delta < 0.5$ pl-as-rhombi bond off-edge with the bonds closer to the small rhombi angle, while for $\Delta > 0.5$ pl-as-rhombi bond off-edge with the bonds closer to the big rhombi angle. In contrast, pl-s-rhombi are the same by rotation of π .

Typical snapshots of pl-systems where chains are colored according to their length are reported in figure 3(a). In the following, we characterize the emerging chains at different ϵ - and Δ -values according to their typical length, packing abilities, nematic order parameter, characteristic bond angle distribution and end-to-end distance (see figures 3 and 4, together with figures 3 and 4 in the supporting information (stacks.iop.org/JPhysCM/32/204001/mmedia)).

3.1.1. Chain length. The average chain length, $\langle L \rangle$, is defined as the average number of monomers in a chain. In all pl-systems, $\langle L \rangle$ increases as the interaction strength ϵ rises (see figure 3(b)): for all pl-types and Δ -values, the formation of chains longer than three particles occurs at $\epsilon = 7.2k_B T$. At $\epsilon = 8.2k_B T$, pl-systems become distinguishable: chains of pl-as tend to be significantly longer than the other types with $\langle L \rangle = 16.92 \pm 0.75$ at $\Delta = 0.8$, in contrast to $\langle L \rangle = 10.53 \pm 0.39$ for pl-center and $\langle L \rangle = 7.02 \pm 0.21$ for pl-s at $\Delta = 0.8$. Additionally, pl-as chains with $\Delta < 0.5$ are notably shorter than chains with $\Delta > 0.5$. It is worth noting that the chain length in pl-systems appears to be distributed exponentially (see the inset of figure 3(b)) and thus the error bars were calculated using the standard error of the mean.

3.1.2. Packing. For all pl-systems, the average packing fraction $\phi = N/[(L_x L_y)l^2 \sin(\alpha)]$ grows on increasing ϵ (see figure 3(c)) and it is relatively symmetric with respect to $\Delta = 0.5$ (corresponding to pl-center). For $\epsilon \leq 7.2k_B T$, we find that ϕ does not depend on the chain type nor on the patch positions, but it is determined only by ϵ . In contrast, at $\epsilon = 8.2k_B T$, when particles start to form longer and longer chains, ϕ increases significantly and it becomes dependent on both the chain type and Δ . At this high energy level, the best packing is achieved

by the linear chains of pl-center with $\phi = 0.61 \pm 0.02$, as they are able to align seamlessly. As patches move off-center, the staggered chains of pl-s (pink line in figure 3(c)) are harder to fit together with respect to the linear chains, resulting in a lower packing fraction that reaches $\phi = 0.49 \pm 0.01$ at $\Delta = 0.2$. The jagged chains in pl-as (purple line in figure 3(c)) align better than the staggered chains, with a packing fraction that is still—but less dramatically—dependent on Δ with $\phi = 0.57 \pm 0.01$ at $\Delta = 0.2$. We observe that the packing of jagged chains with small angle bonds is comparable to the packing of jagged chains with big angle bonds.

3.1.3. Nematic order parameter. While for $\epsilon \leq 7.2k_B T$ (corresponding to low-intermediate packing) the orientations of neighboring chains are independent of each other, at $\epsilon = 8.2k_B T$, chains in all pl-systems tend to align with their neighboring ones. We calculate the fraction of chains in the largest orientationally ordered cluster and the degree of orientational—nematic—ordering within the largest cluster (see section 2.1 of the supporting information). We conclude that all pl-systems pack as nematic fluids, as the fraction of chains in the largest cluster, f_{largest} , typically lies above 0.4 and the nematic order of these largest clusters is $S_{\text{largest}} \approx 0.6\text{--}0.85$ (see figure 3 of the supporting information).

3.1.4. Bond angle distribution. Another way to characterize the emerging chains is the bond angle distribution between neighboring chain elements (see figure 4(a)) [2]. The bonding scenarios can be classified according to the sequence of bond-types along a subchain of three particles. As linear (pl-center, blue histograms in figure 4(a)) and jagged (pl-as, green histogram in figure 4(a)) chains are connected with only one type of bond (on-edge and off-edge p-bonds, respectively), the characteristic bond angles of these systems are close to 0° . The corresponding bonding scenarios are p-p-on (two on-edge p-bonds) for linear chains and p-p-off (two off-edge p-bonds) for jagged chains, where p-p-off bond angles have a slightly broader distribution with respect to p-p-on. In contrast, bond angles of staggered chains (pl-s, red histogram in figure 4(a)) are distributed around three characteristic angles corresponding to three possible bonding scenarios: p-p-on, p-off&p-on (one off-edge and one on-edge bond) and p-p-off.

While the characteristic p-p-on bond angle distribution is independent of Δ and always peaked around 0° , the distributions of p-off&p-on and p-p-off bond angles are dependent on Δ (see figure 4 of the supporting information). At $\Delta = 0.8$ (see again figure 4(a)), p-off&p-on is peaked around 30° and p-p-off is peaked around 55° . It is important to stress that both the bond angle distributions for off-center systems are significantly wider than for pl-center. This effect is a direct result of the higher bond flexibility of off-center bonds, which we find to rise monotonically the more off-center Δ becomes. We further study the bond-flexibility by calculating the bonding entropy for all pair configurations as well as the average bend of a chain and its bend range. We define the bonding entropy as the volume of states of a bonded configuration calculated by MC-simulation of two particles in the NVT ensemble (see section 1 of the supporting information); the average bend of a chain is defined as the mean of the difference in orientation between neighboring chain elements, while the bend range is defined as the standard deviation of the average bend (see section 2.2 of the supporting information). In general, the more-off center Δ is, the higher the bonding entropy, the average bend and the bend range. For further details and results see figures 1, 2 and 5 of the supporting information.

3.1.5. End-to-end distance. The flexibility of a whole chain can be measured by comparing the end-to-end distance l_e , calculated as the distance between the centers of the first and the last particle in the chain, and the contour length l_c , which is the length of the chain when maximally stretched. Note that the maximum stretch is reached when mutual rhombi edges are parallel and the patches are at the maximum distance $2r_p$. The contour length l_c is then given as the distance vector of the sum of all bond vectors corresponding to this maximum stretch and can be calculated analytically. The bond vectors, referred to as \mathbf{v}_{\max} in the following, are dependent on the bond configuration and on Δ . For on-edge bonds (p-on) $\mathbf{v}_{\max,\text{on}}$ is constant across all values of Δ with

$$\mathbf{v}_{\max,\text{on}} = \begin{pmatrix} l + 2r_p \\ 0 \end{pmatrix}. \quad (1)$$

For off-edge bonds (p-off) \mathbf{v}_{\max} depends on Δ and on whether the bond is closer to the small internal rhombi angles (p-off-s) or to the big angles (p-off-b). For p-off-s $\mathbf{v}_{\max,\text{s}}$ is given as

$$\mathbf{v}_{\max,\text{s}}(\Delta) = \begin{pmatrix} l + 2r_p + \cos(\alpha)|l - 2\Delta| \\ \sin(\alpha)|l - 2\Delta| \end{pmatrix}, \quad (2)$$

while for p-off-b we get

$$\mathbf{v}_{\max,\text{b}}(\Delta) = \begin{pmatrix} l + 2r_p - 2\cos(\alpha)|l - 2\Delta| \\ -\sin(\alpha)|l - 2\Delta| \end{pmatrix}. \quad (3)$$

It is important to note that in pl-center systems, rhombi only bond with $\mathbf{v}_{\max,\text{on}}$, while in pl-as systems, rhombi always bond with the same Δ -dependent bond vector, either $\mathbf{v}_{\max,\text{s}}$ (when $\Delta < 0.5$) or $\mathbf{v}_{\max,\text{b}}$ (when $\Delta > 0.5$). In contrast, in pl-s systems all three bond types (p-on, p-off-s, p-off-b) can occur within the same system. Hence, the general expression for

calculating the contour length l_c for a particular chain is the following:

$$l_c = N_{\text{on}}|\mathbf{v}_{\max,\text{on}}(\Delta)| + N_{\text{off-s}}|\mathbf{v}_{\max,\text{s}}(\Delta)| + N_{\text{off-b}}|\mathbf{v}_{\max,\text{b}}(\Delta)|, \quad (4)$$

where N_{on} denotes the number of p-on bonds, $N_{\text{off-s}}$ is the number of p-off-s bonds and $N_{\text{off-b}}$ the number of p-off-b bonds.

The average fraction $\langle l_e/l_c \rangle$ as a function of the chain length L is a measure of the chain flexibility, where $\langle l_e/l_c \rangle = 1$ is the rigid chain limit. For all pl-systems we observe a monotonous increase of $\langle l_e/l_c \rangle$ with L , i.e. the longer the chains, the less flexible they are (see figure 4(b)). In pl-center and pl-as systems, all $\langle l_e/l_c \rangle$ -curves lie on the top of each other for all Δ -values, meaning that these systems possess a comparable, Δ -independent flexibility. In contrast, for pl-s systems $\langle l_e/l_c \rangle$ -curves are dependent on Δ : as soon as Δ departs from the central value, we observe lower $\langle l_e/l_c \rangle$ -values at fixed L in the whole L -range, meaning that the more off-center Δ is, the more flexible the chains are.

3.2. Cluster types in ma/mo-systems

Visual inspection of simulation snapshots shows that in ma- and mo-systems not only chains, but also loops and micelles emerge. In ma-systems, micelles (or minimal loops) consist of three np-bonded particles (referred to as boxes, see clusters labeled as i in figure 5), while in mo-systems they consist of five or six np-bonded particles (referred to as 5- or 6-stars, respectively; see clusters labeled as n and p in figure 5, respectively). The relative abundance of chains, loops and micelles depends on Δ and ϵ , but the small cluster analysis reported in figure 5 allows us to already discern which clusters are allowed, i.e. fulfill the given bonding constraints. These constraints follow from the patch configuration (ma- versus mo-systems), the patch topology (s- versus as-topology) and Δ .

In general, s-topologies with $\Delta < 0.5$ do not allow for p-bonds in clusters bigger than two or three because of bonding incompatibilities (see the relative top-left panels in figure 5). Therefore, in both ma- and mo-systems neither chains nor loops are possible when $\Delta < 0.5$, rendering micelles the only self-assembly product. When $\Delta \geq 0.5$, chains and loops can form because the patch positioning allows for both p- and np-bonds in clusters bigger than two (see the relative bottom-left panels in figure 5). In contrast, we find no such bonding restrictions for as-topologies, and hence chains, loops and micelles are allowed at all Δ -values (see the relative top/bottom-right panels in figure 5). For additional insight into the variety of emerging clusters, the naming of characteristic dimers and trimers is reported in figure 2. Note that due to the np-off-edge bonding of dimers, micelles in ma-as and mo-as have a hole in the center (for both $\Delta < 0.5$ and $\Delta > 0.5$); we refer to the resulting clusters as open boxes and open (5- or 6-) stars.

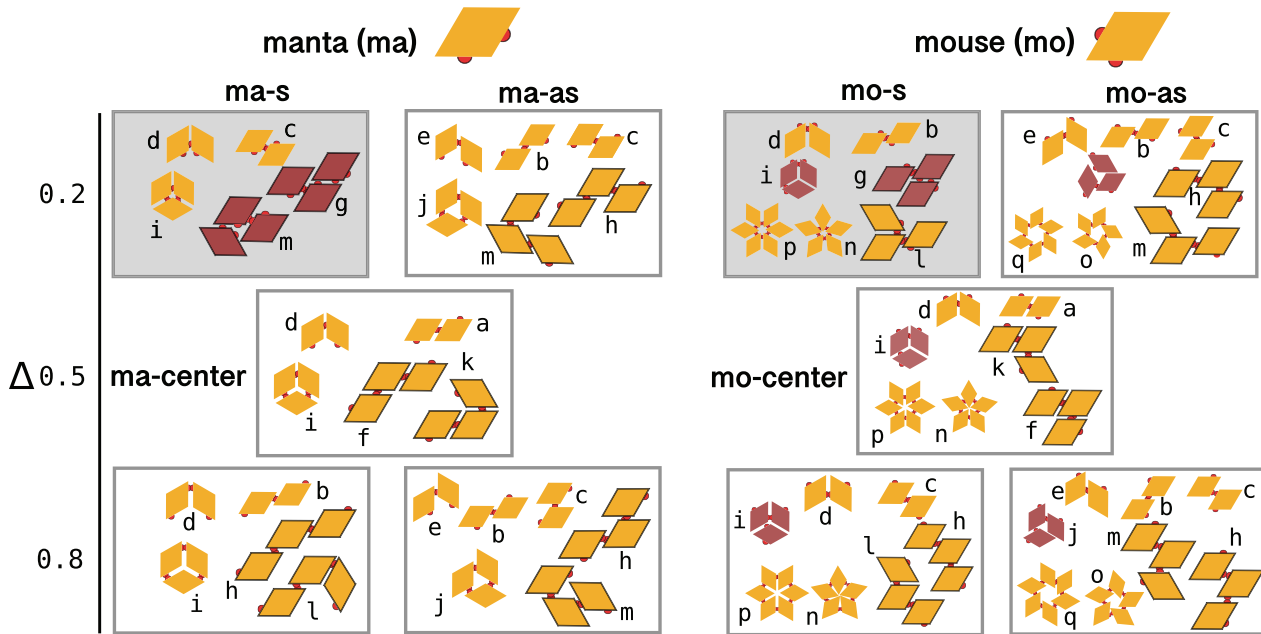


Figure 5. Small cluster analysis for manta (ma) and mouse (mo) systems. For each system type (ma on the left, mo on the right, as labeled) there are two columns, one for symmetric (s) topologies and one for asymmetric (as) topologies, as labeled. The rows correspond to different Δ -values: $\Delta = 0.2$ (top), 0.5 (center) and 0.8 (bottom), as labeled. Note that at $\Delta = 0.5$, s-topologies and as-topologies collapse to the center-topology (all patches are on the edge center). Clusters with fully bonded rhombi are colored in orange, while clusters with non-satisfied bonds are colored in burgundy. Systems that do not yield chains are greyed out. The labeling of the different clusters is summarized in the glossary of figure 2. Note that, while we report all possible dimers, the depicted trimers are just examples of how the available bonding patterns at the two-particle level can be combined; (open) boxes and stars are reported as they are the only possible micelles, i.e. minimal loops, that form in ma- and mo-systems, respectively.

As we are interested in the assembly of chain-like aggregates, we search for the conditions that favor the predominance of chains over loops and micelles. To do so, we calculate yields of cluster types. In ma-systems, we classify clusters of size $L < 3$ as liquid, micelle clusters with $L = 3$ as boxes and non-micelle clusters of size $L \geq 3$ as chains/loops. In mo-systems, clusters with $L < 5$ are liquid, micelle clusters with $L = 5$ are 5-stars/open 5-stars, micelle clusters with $L = 6$ are 6-stars/open 6-stars and non-micelle clusters with $L \geq 5$ are chains/loops. The yield of a cluster type is defined as the percentage of particles that are part of clusters belonging to the selected cluster type. The obtained yields are summarized in figures 6(a) and (b) for ma-systems and in figures 7(a) and (e) for mo-systems. Through a mapping to a barycentric coordinate system (see section 3.1 of the supporting information), we obtain the dominant cluster type at each Δ . The resulting heatmaps are displayed in figures 6(c) and (e) for ma-systems and in figures 7(d) and (f) for mo-systems. Note that in section 3.3 and figure 7 of the supporting information we discuss and show histograms at selected Δ -values where chains and loops are distinguished.

From figures 6(a) and (c), we observe that in ma-s systems, boxes are the dominant cluster type for $\Delta < 0.5$ with yields above 0.9 , as bonding constraints do not allow chains. For ma-center, the box yield drops to 0.204 ± 0.026 , while the chain yield is 0.746 ± 0.0234 and the loop yield is 0.049 ± 0.011 (see figure 7 in the supporting information for yield distributions where chains and loops are distinguished). Moving to

higher Δ , we observe that the box yield is minimal at $\Delta = 0.5$ and $\Delta = 0.6$ and then rises again to reach 0.492 ± 0.032 at $\Delta = 0.8$. In ma-as systems (see figures 6(d) and (e)), we find chains to be the dominant cluster type for all Δ -values. Furthermore, we observe the yields to be independent of Δ for all cluster types, with a chain yield of ≈ 0.75 , a open box yield of ≈ 0.2 and a loop yield of ≈ 0.05 (see again figure 7 in the supporting information).

In mo-s systems (reported in figures 7(a) and (d)), stars are the prevalent cluster type for $\Delta < 0.5$ where 5-stars are dominant at $\Delta = 0.2$ with a yield 0.837 ± 0.041 and 6-stars are dominant at $\Delta = 0.3$ and 0.4 with a yield of 0.580 ± 0.031 and 0.554 ± 0.044 , respectively. For mo-center, chains are dominant with a yield of 0.976 , while the 6-star yield is only 0.024 and loops are not present (figure 7 in the supporting information). For $\Delta > 0.5$, mo-s chains remain the most prevalent cluster type with a yield over 0.95 , while the star yield remains below 0.05 . In contrast to mo-center, when $\Delta > 0.5$ loops are present but with yields of below 0.05 (figure 7 in the supporting information). In mo-as systems (reported in figures 7(e) and (f)), chains are the dominant cluster types at all Δ -values with yields above 0.95 and (almost) independent of Δ . Open stars and loops only reach yields below ≈ 0.05 .

We conclude that for both ma- and mo-systems, the s-topology favors micelles when $\Delta < 0.5$ and chains/loops for $\Delta \geq 0.5$, while the as-topology favors chains/loops over the whole Δ -range. Moreover, when micelles are disfavored, chains prevail over loops. We now focus on the regimes where

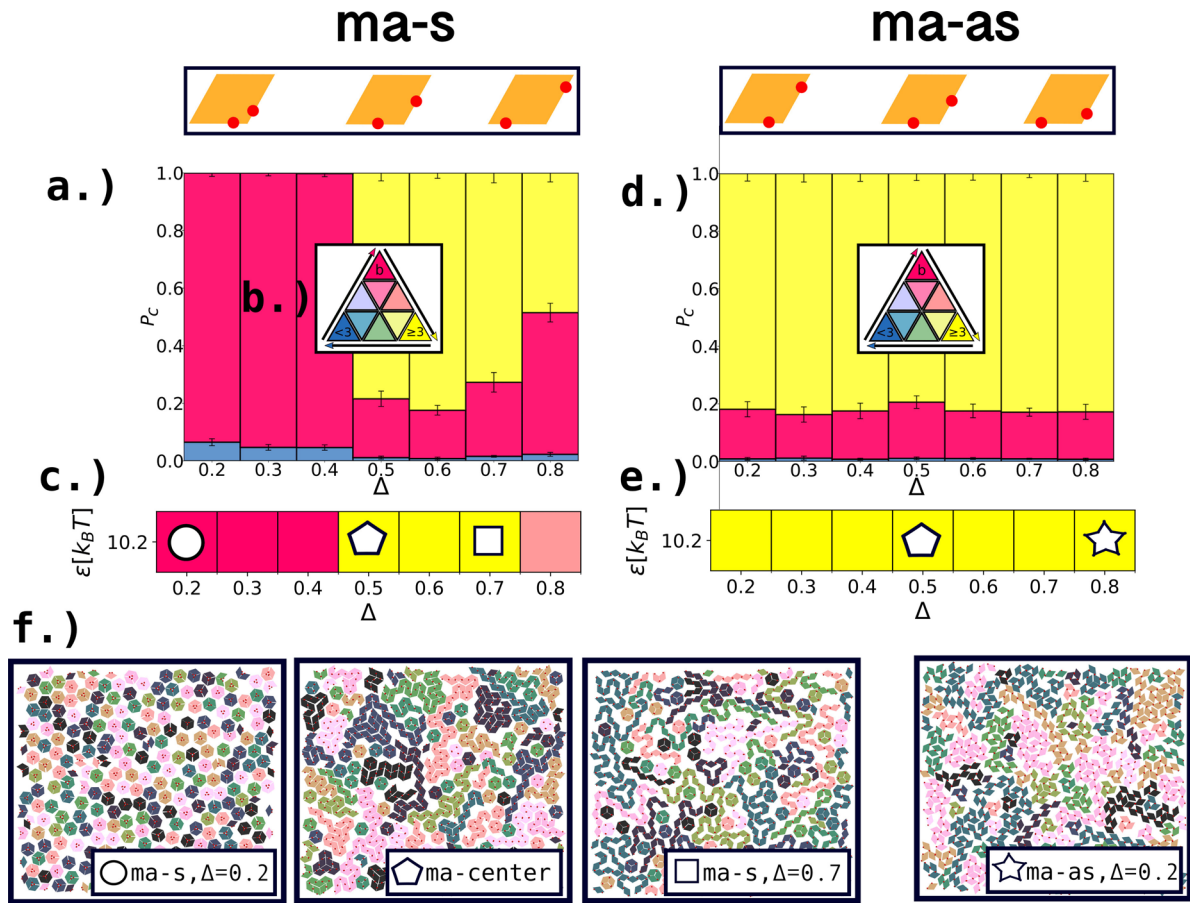


Figure 6. Self-assembly products of ma-systems. Top: sketches of ma-s systems (left panel) and ma-as systems (right panel) with (from left to right in both panels) $\Delta = 0.2, 0.5$ and 0.8 . (a) Histogram of yields for ma-s systems at $\epsilon = 10.2k_B T$ for clusters types of interest: clusters with size $L < 3$ (liquid state, blue), boxes (micelles, pink) and clusters with size $L \geq 3$ (chains/loops, yellow). (b) The barycentric color triangle maps the yields for these cluster types to the heatmap in (c). (d) Histogram of yields for ma-as systems at $\epsilon = 10.2k_B T$ for clusters types of interest: clusters with sizes $L < 3$ (liquid state, blue), open boxes (micelles, purple), and clusters with $L \geq 3$ (chains/loops, yellow). The same barycentric color triangle as in (b) maps the yields for these cluster types to the heatmap in (e). (f) Snapshots of ma-systems (from left to right): ma-s $_{\Delta=0.2}$, ma-center, ma-s $_{\Delta=0.7}$, ma-as $_{\Delta=0.2}$; the color of the clusters is a guide to the eye to distinguish between different close-by aggregates.

chains are dominant and characterize the emerging aggregates. As the snapshots reported in figures 6(f) and 7(g) suggest chains in different systems have different features.

3.3. Chains in ma/mo-systems

The emerging chains in ma- and mo-systems differ from each other with respect to their bonding pattern and therefore also with respect to their appearance and physical properties. From the visual analysis of simulation snapshots (reported in figures 6(f) and 7(g)), we can already infer some characteristic features which distinguish the chains emerging in the different systems. In ma-center and ma-s (with $\Delta > 0.5$), the constraints imposed by on-edge p-bonds and off-edge np-bonds are such that the rhombi tend to turn their vertices with the large angles outward, giving ma-center and ma-s chains a pipe-like appearance. In ma-as on the other hand, rhombi bind exclusively off-edge (for both p- and np-bonds), resulting in jagged chains, where both, small and large angled vertices stick out. In mo-center and mo-s, the constraints imposed by on-edge p-bonds and off-edge np-bonds are such that the

rhombi turn their vertices with small angles outward, making the chains spike-like in appearance. In mo-as, again p- and np-bonds are both off-edge, thus leading to jagged chains.

Similar to the analysis of pl-systems, also for ma- and mo-systems we characterize the emerging chains at different Δ -values (note that for ma- and mo-systems $\epsilon = 10.2k_B T$) according to their typical length, their packing abilities, and their characteristic bond angle distribution (see figures 8 and 9, as well as figure 6 in the supporting information). Note that we neither show the nematic order parameter analysis nor the end-to-end distance as the kinks that characterize the emerging chains do not allow for a meaningful definition of the chain backbone.

3.3.1. Chain length. In both ma- and mo-systems chain lengths appear to be distributed exponentially (see figure 8(b)). Additionally average chain lengths increase or decrease as a function of Δ , symmetrically with respect to $\Delta = 0.5$ (see figure 8(a)). In ma-center, chains have an average length of $\langle L \rangle = 12.97 \pm 0.46$. In ma-s (with $\Delta > 0.5$), the chain length decreases monotonically with Δ and for $\Delta = 0.8$ the average

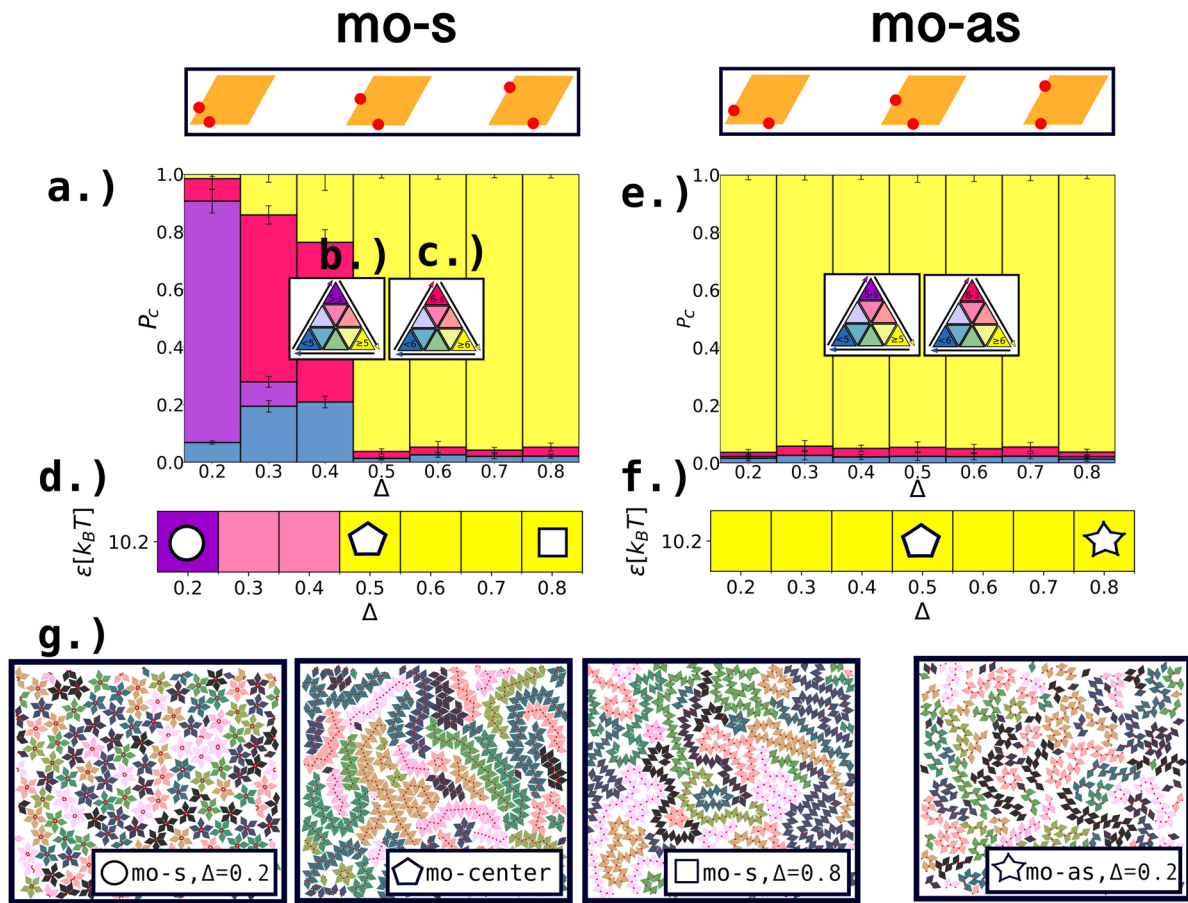


Figure 7. Self-assembly products of mo-systems. Top: sketches of mo-s systems (left panel) and mo-as systems (right panel) with (from left to right in both panels) $\Delta = 0.2, 0.5$ and 0.8 . (a) Histogram of yields for mo-s systems at $\epsilon = 10.2k_B T$ for clusters types of interest: clusters with sizes $L < 5$ (liquid, blue), 5-stars (micelles of five particles, purple), 6-stars (micelles of six particles, pink) and non-micelle clusters with sizes $L \geq 5$ (chains/loops, yellow). (b) The barycentric color triangle maps the yields for the cluster types liquid state (blue), 5-stars (purple) and chains/loops (yellow) for the patch position $\Delta = 0.2$ to the heatmap in (d). (c) The barycentric color triangle maps the yields for the cluster types liquid (blue), 6-stars (pink) and chains/loops (yellow) for $\Delta > 0.2$ to the heatmap in (d). (e) Histogram of yields for mo-as systems at $\epsilon = 10.2k_B T$ for clusters types of interest: clusters with sizes $L < 5$ (liquid state, blue), open 5-stars (micelles of five particles, purple), open 6-stars (micelles of six particles, pink) and non-micelle clusters with $L \geq 5$ (chains/loops, yellow). The barycentric color triangle in (b) maps the yields for the cluster types liquid state (blue), open 5-stars (pink) and chains/loops (yellow) for the patch position $\Delta = 0.2$ to the heatmap in (f). The barycentric color triangle in (c) maps the yields for the cluster types liquid state (blue), open 6-stars (pink) and chains/loops (yellow) for $\Delta > 0.2$ to the heatmap in (f). (g) Snapshots of mo-systems (from left to right): mo-s $_{\Delta=0.2}$, mo-center, mo-s $_{\Delta=0.8}$, mo-as $_{\Delta=0.2}$; the color of the clusters is a guide to the eye to distinguish between different close-by aggregates.

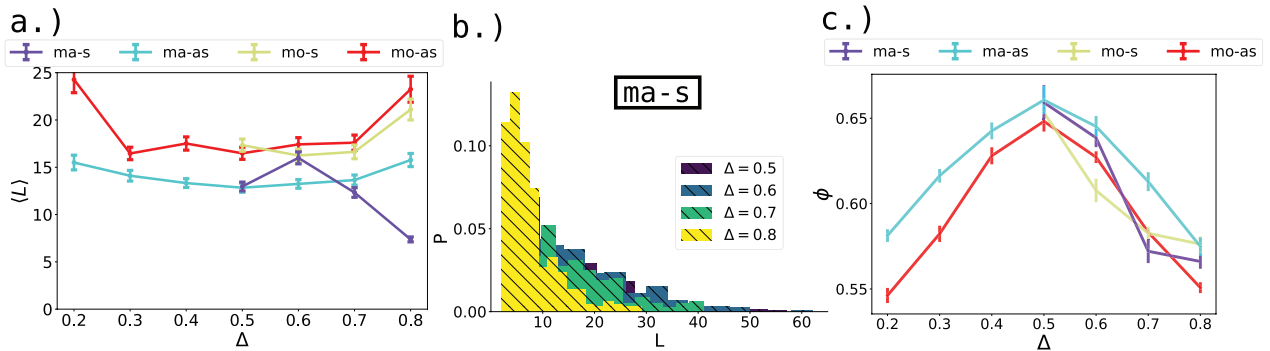


Figure 8. (a) The average chain length $\langle L \rangle$ as a function of Δ for both ma- and mo-systems, (b) Cluster size distribution of ma-s, (c) The packing fraction ϕ as a function of Δ for both ma- and mo-systems.

chain length is $\langle L \rangle = 7.37 \pm 0.26$. In ma-as, on the other hand, the chain length increases monotonically with Δ and it is $\langle L \rangle = 15.76 \pm 0.69$ for $\Delta = 0.8$. In mo-center, chains

have an average length of $\langle L \rangle = 17.33 \pm 0.64$ and in both mo-s and mo-as chains increase with respect to mo-center, and reach $\langle L \rangle = 21.10 \pm 1.10$ at $\Delta = 0.8$ for mo-s and

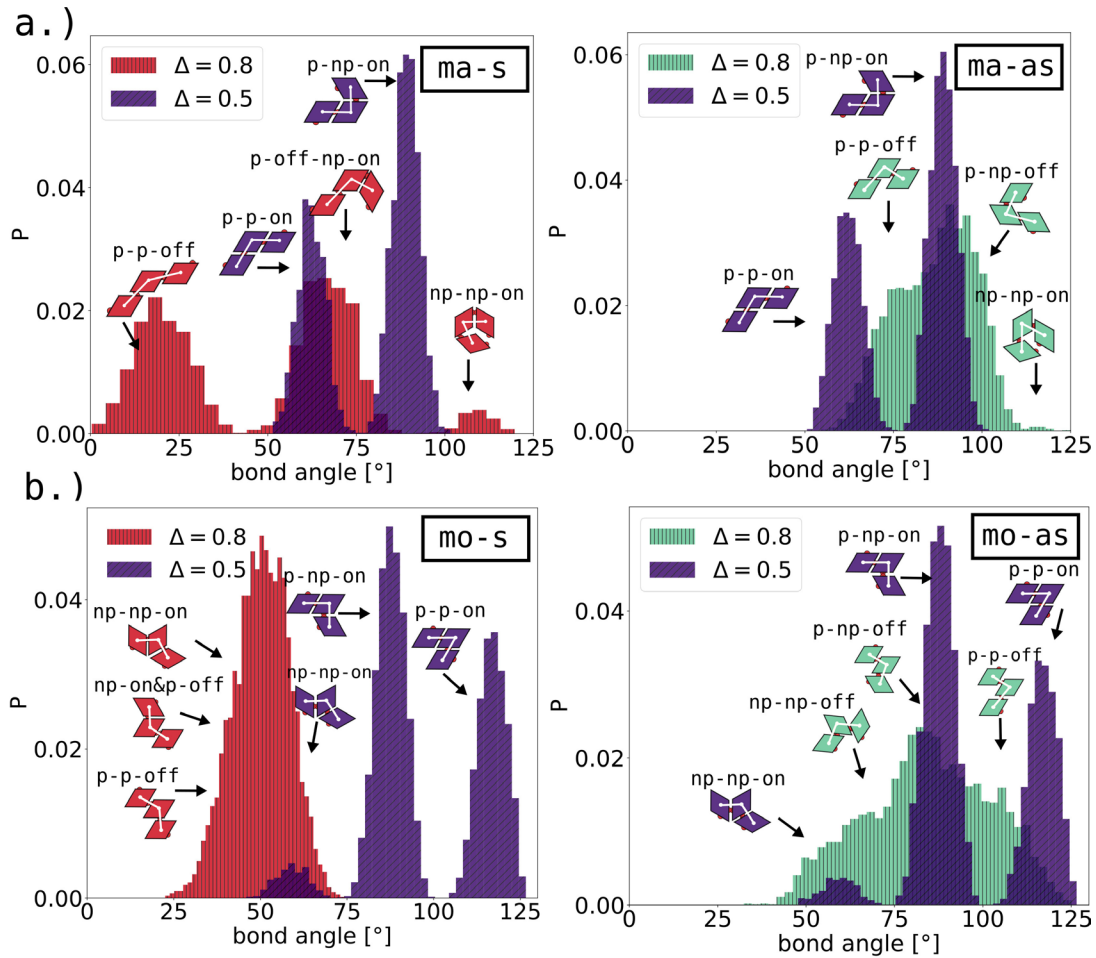


Figure 9. (a) Bond angle distributions for ma-center (blue), ma-s (red) and ma-as (green). Sketches of bonding configurations corresponding to the peaks are added in corresponding colors. The naming scheme of such configurations takes into account if bond are parallel or non-parallel as well as if bonds are on- or off-edge, namely ‘p-p’: two parallel bonds; ‘p-np’: one parallel and one non-parallel bond; ‘np-np’: two non-parallel bonds; ‘on’: on-edge bonds, ‘off’ off-edge bonds. (b) Bond angle distributions for mo-center (blue), mo-s (red) and mo-as (green). Sketches of bonding configurations are added in corresponding colors. The naming scheme is the same as in panel (a).

$\langle L \rangle = 23.25 \pm 1.37$ for mo-as. We can conclude that, in mo-systems chains emerge that are on average longer than those in ma-systems, the longest chains emerging in both cases at extreme Δ -values for the asymmetric topology (jagged chains). On the other hand, the shortest chains are observed for ma-s systems at $\Delta = 0.8$ (pipe-like chains).

3.3.2. Packing. As a general rule, the packing fraction for ma- and mo-center is higher than for their respective off-center topologies (see figure 8(c)). This is due to the fact that when patches are placed on the edge center only on-edge bonds can form (either p- or np-ones), which enables the chains to fit into each other easily, leading to a high packing fraction of $\phi = 0.659 \pm 0.010$ for ma-center and 0.648 ± 0.006 for mo-center. Since the bonding becomes more off-edge as Δ becomes more extreme, the packing fraction goes down monotonously from $\Delta = 0.5$, at $\Delta = 0.8$ $\phi = 0.566 \pm 0.004$ for ma-s, $\phi = 0.575 \pm 0.005$ for ma-as, $\phi = 0.576 \pm 0.004$ for mo-s and $\phi = 0.550 \pm 0.003$ for mo-as. While the best packing is achieved by ma-as-systems over the whole Δ -range, the worst packing is not associated to a specific system.

3.3.3. Bond angle distribution. Bond angles are dependent on the possible bonding configurations within one particle class (pl, ma, mo), on the topology (s, as) and on the value of Δ . In both ma- and mo-systems, three bonding configurations are possible: p-p (two parallel bonds), p-np (one parallel and one non-parallel bond) and np-np (two non-parallel bonds). Additionally, depending on the particle class and on Δ , we find on- or off-edge bonds, the last ones of two-types: p-off-s and p-off-b.

The set of possible bond-angles determines the kinks in the backbone and therefore also system properties, such as packing fraction and average chain length. Each of the investigated systems is characterized by a unique bond angle distribution (see figure 9).

For ma-center the bond-angle distribution is bimodal (see figures 9(a) and (b)) with one peak at 60° (p-p-on bonding) and one at 90° (p-np-on). The on-edge bond together with the sharp angles, give ma-center chains the appearance of double stranded chains (see the corresponding snapshot in figure 6(f)). In ma-s, where we increase Δ symmetrically off-center, the p-p-off and np-on&p-off peaks are shifted to smaller angles

compared to the on-edge bonds of ma-center (see the red histogram in figure 9(a)). Additionally, we observe a third peak, the np-np-on peak at $\approx 110^\circ$, which represents boxes with one broken bond. The off-edge bonding gives ma-s chains the appearance of single stranded chains (see the corresponding snapshot in figure 6(f)). In ma-as, the p-p-off and the np-np-off peak shift and spread into each other to form one diffuse mode. Similar to ma-s, we find np-np-off configurations, i.e. open boxes with one broken bond (see the green histogram in figure 9(a)).

In mo-center, we observe a bond angle distribution with three peaks, the p-p-on at 120° , the p-np-on at 90° and the np-np at 60° (see the blue histogram in figure 9(b)). The on-edge bonds, combined with the sharp bond-angles gives mo-center a double stranded appearance (see the corresponding snapshot in figure 7(g)). In mo-s, as Δ is moved symmetrically off-center, all three peaks merge into one, at $\approx 50^\circ$ for $\Delta = 0.8$ (see the red histogram in figure 9(b)). In mo-as, as Δ is moved asymmetrically off-center, we observe that the three peaks extend into each other, forming one diffuse mode at $\Delta = 0.8$ (see the green histogram in figure 9(b)).

In all systems, the spread of the distributions widens the more off-center Δ becomes. This wider spread is directly related to the fact that the average bend and bend range rise as Δ moves off-center, which in itself originates from the higher bond entropy of off-center pair configurations (see figure 6 in the supporting information for plots of average bend and bend range in ma/mo-systems and section 1 of the supporting information for a calculation of the bonding entropy).

4. Conclusion

In this paper we explore the formation of chains emerging in systems of rhombic platelets decorated with two mutually attractive patches on distinguished edges. We consider the effect of the patch interaction strength and of the patch arrangement—quantified by a patch topology (either symmetric or asymmetric) and a patch position parameter, Δ —on the emerging particles assemblies. For patches placed on opposite edges (referred to as parallel patchy rhombi), chains are the only possible assembly product and they emerge at all the investigated interaction strengths, for both topologies, at all Δ -values. When patches are placed on adjacent edges (either around the big or the small angle, referred to as manta and mouse patchy rhombi, respectively), chains emerge only at high interaction strengths, where a competition between chains and loops is observed. In the case of—with respect to their common vertex—symmetrically placed patches, chains and loops are only allowed when $\Delta \geq 0.5$. In contrast, for asymmetrically placed patches chains and loops form for all Δ -values.

Parallel patchy rhombi form well-defined chains with distinguished properties according to the patch topology: we distinguish between linear, staggered and jagged chains, and these differ in their average length, packing abilities, ordering trends and flexibility properties.

In general, chains of parallel patchy rhombi pack as nematic fluids, with center patch topologies packing better than off-center ones. This is important for a possible second-stage of assembly. Future investigations might focus on the close-packing limit of the different chains and on the percolation properties of these systems, in view of potential applications.

In contrast, chain-like assembly emerging in manta and mouse systems—despite being characterized by average lengths and packing fractions comparable to those observed in parallel patchy rhombi systems and by sharp, characteristic bond angle distributions—cannot be classified as nematic fluids. The flexibility properties of the chains emerging in these systems must be seen in terms of sequences of kinks; depending on the patch positioning the kinks determine the characteristics of the chains.

On a more general level, the choice of the number of patches plays an important role in determining the final assembly products. Recently, we have shown that patchy rhombi with four interaction sites are able to grow extended tilings in two-dimensions [31]. Through choosing particular patch topologies, monolayers can be assembled with identical lattice geometry but different porosity, from a close-packed arrangement to an open lattice. Interestingly, the open lattices observed in [31] result from the second-stage assembly—due to the two additional patches—of the open micelles (both boxes and stars) observed here. A more thorough analysis of micelles is reported in [28].

Finally, comparing our system with current literature we find that one of the—to date—rare works featuring a competition of micelles and tubular structures in assemblies of anisotropic particles is a study of prolate Janus ellipsoids in three dimensions [32]. While for small and large aspect ratios micelles prevail, at intermediate aspect ratios, tubular structures dominate the assembly. In contrast to the boxes and stars in our systems, the rather spherical micelles formed in these systems do not have a fixed number of particles. We argue that it is the localized patches together with the flat edges of patchy rhombi—and possibly of other patchy polygons and polyhedra—that lead to the formation of well defined distinct cluster types. We conclude that in both systems—the two dimensional patchy rhombi and the three dimensional Janus ellipsoids—shape and interaction center anisotropy lead to rich variability in cluster types and shape.

Acknowledgments

CK and EB acknowledge support from the Austrian Science Fund (FWF) under Proj. No. Y-1163-N27. Computation time at the Vienna Scientific Cluster (VSC) is also gratefully acknowledged. VMD was used to generate the simulation snapshots [33].

ORCID iDs

Carina Karner  <https://orcid.org/0000-0002-2403-3697>

Emanuela Bianchi  <https://orcid.org/0000-0002-3282-1087>

References

- [1] Liu K, Nie Z, Zhao N, Li W, Rubinstein M and Kumacheva E 2010 *Science* **329** 197
- [2] Vutukuri H R, Demirörs A F, Peng B, van Oostrum P D J, Imhof A and van Blaaderen D A 2012 *Angew. Chem., Int. Ed.* **51** 11249
- [3] Kuei S, Garza B and Biswal S L 2017 *Phys. Rev. Fluids* **2** 104102
- [4] Zöttl A and Yeomans J M 2019 *Nat. Phys.* **15** 554
- [5] Kirchenbuechler I, Guu D, Kurniawan N A, Koenderink G H and Lettinga M P 2014 *Nat. Commun.* **5** 5060
- [6] Vilfan M, Potočnik A, Kavčič B, Osterman N, Poberaj I, Vilfan A and Babič D 2010 *Proc. Natl Acad. Sci.* **107** 1844
- [7] Su M, Li F, Chen S, Huang Z, Qin M, Li W, Zhang X and Song Y 2016 *Adv. Mater.* **28** 1369
- [8] Choueiri R M, Galati E, Klinkova A, Thrien-Aubin H and Kumacheva E 2016 *Faraday Discuss.* **191** 189
- [9] Hu Y, He L and Yin Y 2011 *Angew. Chem., Int. Ed.* **50** 3747
- [10] Demortière A, Snezhko A, Sapozhnikov M V, Becker N, Proslie T and Aranson I S 2014 *Nat. Commun.* **5** 3117
- [11] Bharti B and Velev O D 2015 *Langmuir* **31** 7897
- [12] Pawar A and Kretzschmar I 2010 *Macromol. Rapid Commun.* **31** 150
- [13] Bianchi E, Blaak R and Likos C N 2011 *Phys. Chem. Chem. Phys.* **13** 6397
- [14] Bianchi E, Capone B, Coluzza I, Rovigatti L and van Oostrum P D J 2017 *Phys. Chem. Chem. Phys.* **19** 19847
- [15] Herlihy K P, Nunes J and DeSimone J M 2008 *Langmuir* **24** 8421
- [16] Yanai N, Sindoro M, Yan J and Granick S 2013 *J. Am. Chem. Soc.* **135** 34
- [17] Azari A, Crassous J J, Mihut A M, Bialik E, Schurtenberger P, Stenhammar J and Linse P 2017 *Langmuir* **33** 13834
- [18] Coluzza I, van Oostrum P D J, Capone B, Reimhult E and Dellago C 2013 *Phys. Rev. Lett.* **110** 075501
- [19] Zhao S, Wu Y, Lu W and Liu B 2019 *ACS Macro Lett.* **8** 363
- [20] Yan J, Chaudhary K, Bae S C, Lewis J A and Granick S 2013 *Nat. Commun.* **4** 1516
- [21] Shah A A, Schultz B, Zhang W, Glotzer S C and Solomon M J 2015 *Nat. Mater.* **14** 117
- [22] Rothmund P W K 2006 *Nature* **440** 297
- [23] Xu W, Li Z and Yin Y 2018 *Small* **14** 1801083
- [24] Ye X et al 2013 *Nat. Chem.* **5** 466
- [25] Senyuk B, Liu Q, Bililign E, Nystrom P D and Smalyukh I I 2015 *Phys. Rev. E* **91** 040501
- [26] Golshtein E G and Tretyakov N 1996 *Modified Lagrangians and Monotone Maps in Optimization* (New York: Wiley)
- [27] Whitelam S, Tamblyn I, Beton P H and Garrahan J P 2012 *Phys. Rev. Lett.* **108** 035702
- [28] Karner C, Dellago C and Bianchi E 2019 (arXiv:2001.00373) in preparation
- [29] Whitelam S and Geissler P 2007 *J. Chem. Phys.* **127** 154101
- [30] Whitelam S 2011 *Mol. Simul.* **37** 606
- [31] Karner C, Dellago C and Bianchi E 2019 *Nano Lett.* **19** 7806
- [32] Li W and Gunton J D 2013 *Langmuir* **29** 8517
- [33] Humphrey W, Dalke A and Schulten K 1996 *J. Mol. Graph.* **14** 33